Extracellular vesicles from human cardiac progenitor cells inhibit cardiomyocyte apoptosis and improve cardiac function after myocardial infarction

Lucio Barile[1][*][†], Vincenzo Lionetti[2][†], Elisabetta Cervio[1], Marco Matteucci[2],
Mihaela Gherghiceanu[3], Laurentiu M. Popescu[3], Tiziano Torre[1], Francesco Siclari[1],
Tiziano Moccetti[1], and Giuseppe Vassalli[1,4][*]

[1]Laboratory of Molecular and Cellular Cardiology, Departments of Cardiology and Heart Surgery, Fondazione Cardiocentro Ticino, Via Tesserete 48, CH-6900 Lugano, Switzerland; [2]Laboratory of Medical Science, Institute of Life Sciences, Scuola Superiore Sant'Anna, Pisa, Italy; [3]'Victor' Babes National Institute of Pathology, Bucharest, Romania; and [4]Department of Cardiology, Centre Hospitalier Universitaire Vaudois (CHUV), Lausanne, Switzerland

Aims	Recent evidence suggests that cardiac progenitor cells (CPCs) may improve cardiac function after injury. The underlying mechanisms are indirect, but their mediators remain unidentified. Exosomes and other secreted membrane vesicles, hereafter collectively referred to as extracellular vesicles (EVs), act as paracrine signalling mediators. Here, we report that EVs secreted by human CPCs are crucial cardioprotective agents.
Methods and results	CPCs were derived from atrial appendage explants from patients who underwent heart valve surgery. CPC-conditioned medium (CM) inhibited apoptosis in mouse HL-1 cardiomyocytic cells, while enhancing tube formation in human umbilical vein endothelial cells. These effects were abrogated by depleting CM of EVs. They were reproduced by EVs secreted by CPCs, but not by those secreted by human dermal fibroblasts. Transmission electron microscopy and nanoparticle tracking analysis showed most EVs to be 30−90 nm in diameter, the size of exosomes, although smaller and larger vesicles were also present. MicroRNAs most highly enriched in EVs secreted by CPCs compared with fibroblasts included miR-210, miR-132, and miR-146a-3p. miR-210 down-regulated its known targets, ephrin A3 and PTP1b, inhibiting apoptosis in cardiomyocytic cells. miR-132 down-regulated its target, RasGAP-p120, enhancing tube formation in endothelial cells. Infarcted hearts injected with EVs from CPCs, but not from fibroblasts, exhibited less cardiomyocyte apoptosis, enhanced angiogenesis, and improved LV ejection fraction (0.8 ± 6.8 vs. $−21.3 \pm 4.5\%$; $P < 0.05$) compared with those injected with control medium.
Conclusion	EVs are the active component of the paracrine secretion by human CPCs. As a cell-free approach, EVs could circumvent many of the limitations of cell transplantation.
Keywords	Extracellular vesicles • Exosomes • Cardiac progenitor cells • MicroRNA • Cardioprotection • Apoptosis • Angiogenesis

1. Introduction

Ischaemic heart disease and ensuing heart failure are leading causes of morbidity and mortality worldwide. An extensively investigated approach for ischaemic heart disease is cell transplantation. Multiple cell sources including bone marrow,[1] adipose tissue,[2] skeletal myoblasts,[3] and cardiac progenitor cells (CPCs)[4] have been evaluated in both animal models and humans. Clinical trials of autologous BM cell transplantation in patients after acute myocardial infarction (MI) have provided mixed results, with an overall modest improvement in cardiac function.[5] Intramyocardial injection of CPCs isolated from adult hearts improved cardiac function in animal models of MI.[6−8] Although both direct cell differentiation and indirect mechanisms, such as secreted growth factors and cytokines, have been implicated

* Corresponding author. Tel: +41 91 805 3359; fax: +41 91 805 3323, Email: lucio.barile@cardiocentro.org (L.B.), giuseppe.vassalli@cardiocentro.org (G.V.)
† L.B. and V.L. contributed equally to this work.

in the therapeutic benefit, accumulating evidence suggests predominant roles of the paracrine secretion by CPCs.[8] This concept is supported by the observation that CPC-conditioned medium (CM) protects cardiomyocytes against stress-induced apoptosis, while stimulating tube formation in endothelial cells in vitro.[8–11] The CADUCEUS trial of cardiosphere-derived cells has shown that some degree of cardiac regeneration in injured hearts may be possible. The mechanism of benefit was thought to be indirect.[4]

A key component of paracrine secretion in many cell types are extracellular vesicles (EVs), particularly its exosomal fraction. Exosomes are 40–90 nm-sized particles stored intracellularly in endosomal compartments, which are secreted when these structures fuse with the plasma membrane.[12,13] Conventional surface markers of exosomes include the tetraspanin family members, CD9, CD63, and CD81, among others. Exosomes carry proteins, lipids, and nucleic acids including DNA, mRNAs, and microRNAs (miRNAs), which they can shuttle to recipient cells, even at a distance. miRNAs are 18–25 nucleotide, non-coding RNAs that regulate gene expression through post-transcriptional repression. Transfer of mRNAs and miRNAs through exosomes has emerged as a crucial mechanism of genetic exchange between cells.[14,15] Non-exosomal EVs arise by distinct mechanisms including direct budding from the plasma membrane. While non-exosomal EVs are typically larger than exosomes, exosome purification remains a challenging task. As a result, exosomal preparations used in many studies showed limited purity.[16]

Exosomes were identified as the active component of the proangiogenic paracrine activity of bone marrow CD34$^+$ stem cells.[17] Moreover, exosomes secreted by mesenchymal stem cells (MSCs) and mouse CPCs mitigated tissue damage and ventricular remodelling in animal models of myocardial ischaemia and reperfusion injury.[18,19] However, exosomes secreted by human CPCs have not been characterized yet. Using transmission electron microscopy, we recently provided ultrastructural evidence of exosomes and EVs secretion by human CPCs.[20] Here, we report that EVs are the active component of the paracrine secretion by human CPCs. Transmission electron microscopy and nanoparticle tracking analysis showed most EV secretion by CPCs to be 30–90 nm in diameter, suggesting they were exosomes, although smaller and larger vesicles were also present. Moreover, the purified particles expressed conventional exosomal markers including CD63. These results suggest that exosomes were the predominant component of the particles purified from CM-CPC. To stress their heterogeneity, however, we hereafter refer to them as EVs. These EVs mitigated apoptosis triggered by serum deprivation in the neonatal mouse HL-1 cardiomyocytic cell line, while stimulating tube formation in human umbilical vein endothelial cells (HUVECs), an indicator of angiogenic activity. In vivo, injection of EVs secreted by CPCs into the infarct border zone reduced cardiomyocyte apoptosis and scar, increased both viable mass in the infarct area and blood vessel density, and prevented the early impairment of ventricular function in a rat model of acute MI. EVs secreted by normal human dermal fibroblasts (NHDFs) lacked these beneficial effects, supporting the concept that functional activities of EVs depend on the parent cell.[17] A comparison of the miRNA transcriptional profile of EVs secreted by CPCs with that of EVs secreted by NHDFs identified several miRNAs as being particularly enriched in the former, including miR-210, miR-132, and miR-146a-3p. Because cardioprotective roles of miR-210 and a role for miR-132 in vascular remodelling have been reported,[21,22] we focused on the functional activities of these miRNAs. Both miR-210 and miR-132 protected HL-1 cardiomyocytic cells against apoptosis. In addition, miR-132 promoted the formation of endothelial tube. These results suggest that

EVs secreted by CPCs may impart cardiac protection and the underlying mechanism may involve miRNAs.

2. Methods

2.1 Cell sources

Human right atrial appendage specimens were obtained from patients ($n = 22$) who underwent surgical repair of heart valve disease and had no concomitant coronary artery disease. The study was approved by the local Ethical Committee and performed according to the Declaration of Helsinki. All patients gave written informed consent to the collection of atrial specimen. Using the primary ex vivo tissue culture technique,[6–8] the cellular outgrowth of atrial explants was collected within 14 days and seeded into fibronectin-coated 25 mL flasks. EVs were purified from CPCs after two passages in culture. NHDFs were purchased from Life Technologies.

2.2 EV purification methods

Medium conditioned by CPCs (CM-CPC) or NHDFs was obtained by culturing cells in basal medium (BM), a 1 : 1 mix of Iscove's Modified Dulbecco's Media and Dulbecco's Modified Eagle's Medium (Gibco) supplemented with 1% human serum albumin, for 48 h, followed by centrifugation at 3000 g for 15 min, filtration through a 0.2 μm membrane (BD Biosciences), and processing using one of the following methods: (i) ExoQuick^{TM} precipitation solution (System Biosciences; SBI); (ii) ultracentrifugation at 100 000 g for 90 min; and (iii) column precipitation using Exo-spin^{TM} kits (Cell Guidance Systems, Cambridge, UK). The EV pellet was re-suspended in 100–500 μL of phosphate-buffered saline (PBS; pH 7.4) and stored at −80°C. Nanoparticle tracking analysis was performed using NanoSight LM10 (Malvern Instruments, Worcestershire, UK). CD63 and CD81 protein levels in EVs were determined by western blotting. Protein lysate was obtained by re-suspending EV pellet in 100 μL of RIPA buffer (Sigma). Antibodies were purchased from SBI. Total proteins were measured using BCA kits (Thermo Fisher Scientific).

2.3 Transmission electron microscopy

The ultrastructure of EVs was analysed using transmission electron microscopy, as described previously.[23] Briefly, re-suspended EV pellet (3 μL) was fixed with 2.5% glutaraldehyde, post-fixed in buffered 1% OsO_4 with 1.5% $K_4Fe(CN)_6$, embedded in 1% agar, and processed according to the standard Epon812 embedding procedure. EVs were visualized on thin sections (60 nm) using a Morgagni 268 transmission electron microscope (FEI Company, The Netherlands) at 80 kV.

2.4 Flow cytometry

Surface markers expressed on CPCs and EVs were analysed by flow cytometry. Microbeads coated with anti-CD63 antibody (Life Technologies) were used in EV analyses. Phycoerythrin (PE)-conjugated antibodies against surface markers expressed on CPCs or MSCs (CD90, CD105, CD140, CD146, CD166, CD172, and NG2 proteoglycan; all from Beckman Coulter) or conventional exosomal markers (CD9, CD63, and CD81; all from BD Biosciences) were used. Beads incubated with an antibody in the absence of EVs served as a control. To assess dynamic trafficking of CD63 to exosomes, CPCs were transfected with pCT-CD63-GFP vector (CytoTracer; SBI) expressing a CD63-GFP fusion, using lipofectamine. Analyses were performed on a MACS-Quant flow cytometer (Miltenyi Biotec).

2.5 EV uptake by HL-1 cardiomyocytic cells

To assess EV uptake by HL-1 cardiomyocytic cells, EVs from CPCs were labelled with DiI. Excess dye was removed by precipitation of EV. Cells cultured in complete Claycomb medium[24] (Sigma), hereafter referred to as growth medium (GM)-FBS, were incubated with DiI-labelled EVs. After 12 h, cells were imaged using a Nikon C2 Plus confocal microscope. RNA

extraction, reverse transcription, and real-time PCR protocols were used as described in Supplementary material online, to determine intracellular concentrations of miR-210 and miR-132 in HL-1 cells exposed to EV-CPC. In the time-course experiment, 100 µg of EV-CPC total protein were used ($n = 3$ experiments). Dose−response study measurements were performed at 48 h ($n = 3$ experiments).

2.6 *In vitro* apoptosis assay

To induce apoptosis in the mouse HL-1 cardiomyocytic cell line, GM-FBS was replaced by BM for 12 h. After 12 h, medium was supplemented with CM-CPC, EV-depleted CM-CPC (DCM), or DCM reconstituted with the previously removed EV fraction (DCM + EV) for 36 h. Cells kept in BM for 48 h or changed to GM-FBS after 12 h served as controls. A pooled sample of purified EVs secreted by CPCs (EV-CPC; $n = 4$ patients) was compared with EVs secreted by NHDF (EV-F). Viable and dead cells were stained using double staining kits (Dojindo EU GmbH, Germany). Activation of apoptotic pathways was detected using activated caspase-3/7 staining kits (Life Technologies).

2.7 *In vitro* angiogenesis assay

To assess the angiogenic potency of CM-CPC, EV-CPC, and EV-F, HUVECs were seeded at 3×10^4 cells/cm^2 density in Matrigel (BD Biosciences). An endothelial cell medium (Medium 200; Gibco) supplemented with 10% FBS (ECM-FBS) served as a positive control. Images were acquired 5 h later, and tube length was measured using the ImageJ software (National Institutes of Health, USA).

2.8 miRNA analyses

Total RNA was isolated from EV-CPC and EV-F using Quanti-miR kits (SBI). Real-time PCR was performed with Advanced SYBR Green kits (Bio-Rad) using a multistep approach. In a first step, 384 miRNAs were measured in total RNA from a pooled EV-CPC sample ($n = 4$ patients) using synthetic 'spike-in' miRNA sequences, provided with the kits for normalization. Fifty-two miRNAs were found to be enriched more than six-fold compared with 'spike-in' miRNA sequences. In the following step, these miRNAs were directly compared with EVs from CPCs and those from NHDFs. Fourteen miRNAs were found to be particularly enriched in EVs from CPCs. These miRNAs were then measured in three pooled EV-CPC samples ($n = 4$ patients each). Based on the results of this analysis, 7 of 14 miRNAs were then measured in EV-CPC samples from individual patients ($n = 6$). Data were normalized for the geometric mean of miR-U6 and RNU-6B values and shown as 2^{-DDCt} values. Among the most highly enriched miRNAs in EVs secreted by CPCs, miR-210 and miR-132 were chosen for functional studies, owing to their proposed roles in cardioprotection and vascular remodelling.[21,22] Cells were transfected with miR-210 and miR-132 mimics, or siRNAs specific for these miRNAs, using RNAiMAX™ (Life Technologies). Expression of the miR-210 targets, ephrin A3, PTP1b, and FLASH/CASP8AP2,[21,25,26] as well as those of miR-132 target, RasGTPase-activating protein (RasGap)-p120,[22] was measured by western blot using antibodies from Santa Cruz Biotech.

2.9 *In vivo* myocardial infarction

Experimental protocols were approved by the Animal Care Committee of the Italian Ministry of Health, in accordance with Italian (DL-116, 27 January 1992) and international laws and policies (European Economic Community Council Directive 86/609, OJL 358, 12 December 1987). Animal studies were performed as previously described.[27] Briefly, acute MI was induced in healthy male Wistar rats (250−300 g body weight), anaesthetized with a cocktail of tiletamine and zolazepam (Zoletil 100, Virbac, France; dosage 40 mg/kg IP), intubated, and ventilated. The left anterior descending coronary artery was permanently ligated near its origin with a 6-0 Prolene suture. After 60 min, the viable myocardium bordering the LV infarct zone was injected at three different sites with a total of 150 µL of one of the following solutions: PBS ($n = 9$), 30 µg of EV-CPC ($n = 9$), 300 µg of EV-CPC ($n = 10$), and 300 µg of Exo-F ($n = 4$). The sham-operated group included nine animals. At Day 7, rats were anaesthetized with Zoletil 100 (40 mg/kg) and sacrificed with iv KCl (1−2 mEq/kg) to induce diastolic arrest of cardiac activity.

2.10 Echocardiography

Echocardiography was performed in rats sedated by IP tiletamine (29 mg/kg) plus xylazine (4.3 mg/kg). Transthoracic echocardiography was performed on Day 2 (baseline) and Day 7 post-MI using the MyLab 30 echocardiography system (Esaote, Italy), equipped with a 12 MHz linear transducer, as described previously.[28] Under electrocardiographic monitoring of heart rate, the hearts were imaged in 2D long-axis views at the level of the highest LV diameter. LV end-diastolic and end-systolic diameters (LVEDD/LVESD), end-diastolic wall thickness (LVEDTHK-BZ) and end-systolic wall thickening in the border zone (LVESTK-BZ), and LV ejection fraction (LVEF) were measured from 2D long-axis views taken through the infarcted area. Changes in LVEF were calculated as LVEF (Day 7) − LVEF (baseline)/LVEF (baseline).

2.11 Histology

Rats were sacrificed at Day 7 after MI. For immunohistochemistry, hearts were cryopreserved in optimal cutting temperature compound (Sigma) at −80°C. For morphometry, they were embedded in paraffin and cut at 8 µm thin sections. Apoptotic cardiomyocytes were detected by TUNEL assay using In Situ Cell Death Detection kits (Roche) and a monoclonal antibody against α-sarcomeric actinin (α-SA; Sigma).[7] From the Masson's trichrome-stained images (HT15 Trichrome Stain kit; Sigma), viable tissue and scar area within the infarct region were measured on each section by tracing the infarct borders manually using the ImageJ software. Six sections were analysed per heart. Newly formed blood vessels were counted as SMA$^+$/isolectin-IB4$^-$ (Sigma) structures under the microscope.

2.12 Statistical analysis

Unless otherwise stated, results are presented as means ± SEM of n independent experiments. Statistical analyses were performed using InStat, version 3.0 (GraphPad Software, Inc.). The assumption that data were sampled from populations with identical SDs was tested using the method of Bartlett. One-way analysis of variance (ANOVA) with subsequent *post hoc* multiple comparison (Tukey−Kramer multiple comparisons test and Kruskal−Wallis test for parametric and non-parametric comparisons, respectively) was performed. Differences with a *P*-value of <0.05 were considered statistically significant.

3. Results

3.1 Exosomes are the predominant component of EVs

Purified particles from CM-CPC using the ExoQuick™ method were studied by transmission electron microscopy and found to be 72.8 ± 20.8 nm in diameter. Many of them exhibited bi-layer membranes (*Figure 1B−B$_I$*). Nanoparticle tracking analyses of purified EVs from CPCs using ExoQuick™, ultracentrifugation, or Exo-spin™ revealed modal particle sizes (range; nm) of 73 nm (40−250), 85 nm (50−400), and 68 nm (40−400), respectively (*Figure 1C−E*), and concentrations ($\times 10^8$ particles/mL) of 9.8, 7.2, and 4.3, respectively. The ExoQuick™ method yielded higher CD63 and CD81 protein levels compared with the other methods (*Figure 1H*). Flow cytometric analyses of EVs secreted by CPCs revealed the expression of conventional exosomal markers (CD63, CD9, and CD81; *Figure 1F* and *G*) along with MSC/stromal markers (CD105, CD90, CD146, CD172, and NG2) also expressed
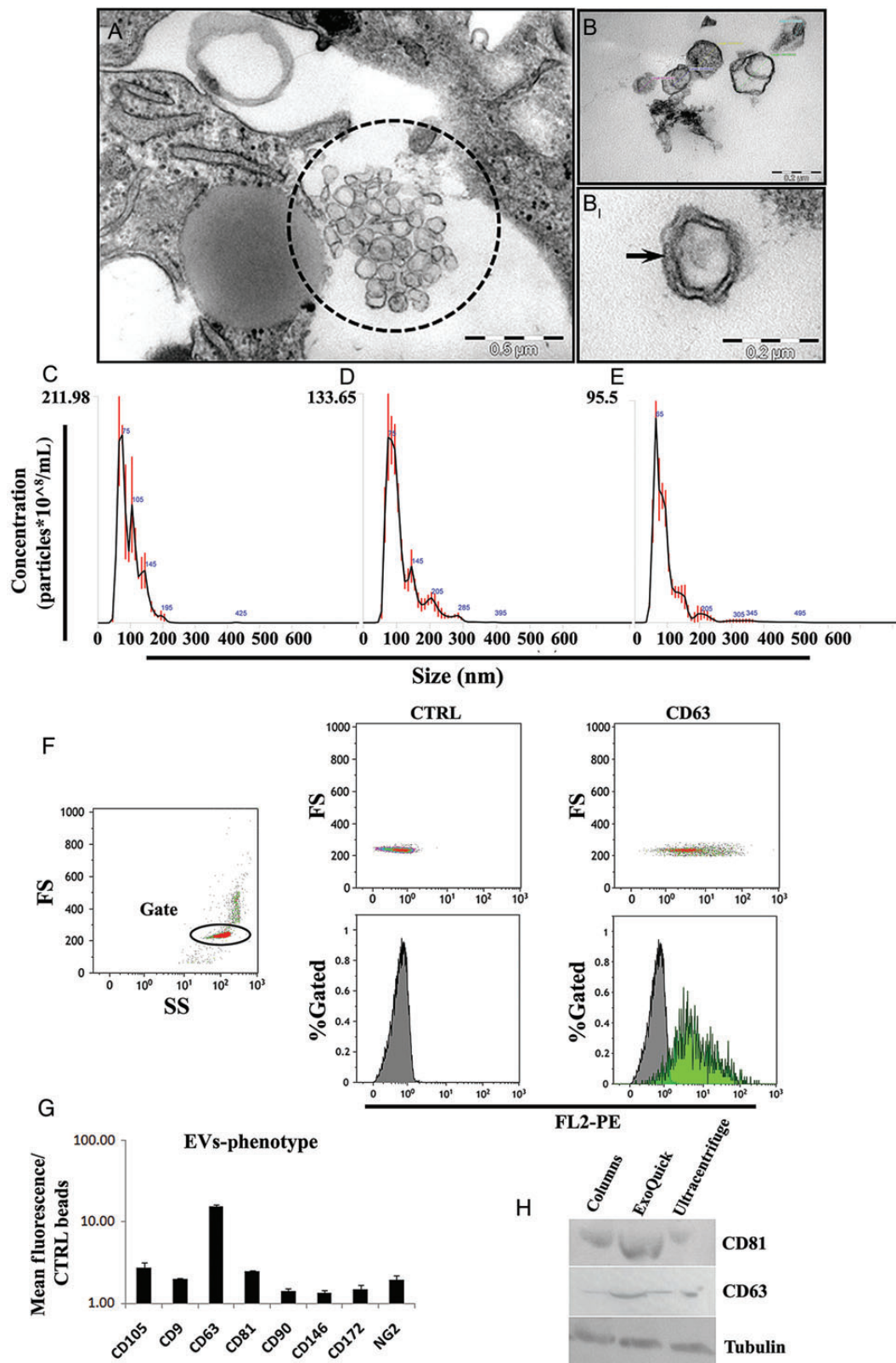
Figure 1 (*A*) Transmission electron micrographs showing EVs (dotted circle) secreted by human CPCs (EV-CPC) in culture. (*B*) Purified EVs showing a characteristic lipid bi-layer membrane (*B*₁: higher-magnification view). (*C*) Nanoparticle tracking analysis of EVs purified using ExoQuick™ precipitation solution. (*D*) EVs purified by ultracentrifugation. (*E*) EVs purified by Exo-spin™ column precipitation. (*F*) Flow cytometric analysis of EVs secreted by CPCs. Left panel: side/forward scatter (SS/FS) plot of CD63-immunobeads in the absence of antibody and EVs; gating on single beads (red dots within the circle; higher FS values are from bead aggregates). Mid panels: control (anti-CD63 antibody; no EVs). Right panels: EVs with PE-conjugated anti-CD63 Ab. (*G*) Quantitative analysis of surface marker expression on EV-CPC (mean ± SEM; $n = 3$ experiments). (*H*) CD63 and CD81 western blots for EV-CPC purified using each of the aforementioned methods.

on parent CPCs (see Supplementary material online, *Figure S1*). Furthermore, dynamic trafficking of CD63 to exosomes was visualized in EVs secreted by CPCs transfected with the CD63-GFP vector (see Supplementary material online, *Figure S2*). Taken together, these results indicate that exosomes are the predominant component of EVs secreted by CPCs. With respect to the degrees of exosomal purity achieved by the three methods used, ExoQuick™ was comparable with, or slightly better than, ultracentrifugation and Exo-spin™. However, a thorough comparison of purification methods was beyond the scope of this study.

3.2 EVs are the active component of CM-CPC

Anti-apoptotic activities of CM-CPC were assessed in the HL-1 cardiomyocytic cell line after 48 h of serum deprivation (*Figure 2A*). CM-CPC added at 12 h reduced dead cells to $40 \pm 8\%$ compared with $72 \pm 9\%$ in the control group ($P < 0.05$; *Figure 2B*). EV-depleted CM-CPC (DCM) did not reduce the number of dead cells ($72 \pm 6\%$; NS). Reconstituting DCM with the previously removed EV fraction (DCM + EV) restored anti-apoptotic activity, reducing dead cells to $44 \pm 5\%$ ($P < 0.05$ vs. BM). Similar changes were found in cells positive for activated caspase-3/7, a marker of programmed cell death activation (*Figure 2C*). Analogously, CM-CPC and DCM + EV, but not DCM, stimulated tube formation in HUVECs (*Figure 2D*). We then compared purified EVs secreted by CPCs with those secreted by fibroblasts. Only the former inhibited starvation-induced apoptosis in the HL-1 cardiomyocytic cell line, while stimulating tube formation in HUVECs (*Figure 3*). These results demonstrate that EVs are the active component of CM-CPC, and that functional activities of EVs depend on the parent cell type.

3.3 EVs secreted by CPCs are taken up by cardiomyocytes and impact on intracellular miRNA concentrations

Using laser confocal microscopy, we provided qualitative evidence that HL-1 cardiomyocytic cells take up DiI-labelled EVs secreted by CPCs (*Figure 4A−F*). miRNA analyses revealed that miRNA-210 and miRNA-132 were among the most highly enriched miRNAs in EVs secreted by CPCs compared with those secreted by fibroblasts (*Figure 4G* and see Supplementary material online, *Figure S3*). Incubation of these cells with EVs from CPCs resulted in a time and dose-dependent increase in the intracellular concentrations of miRNA-210 and miRNA-132 (*Figure 4H*). This observation plausibly reflects EV-mediated miRNA transfer to these cells.

3.4 EVs secreted by CPCs are enriched in miRNAs with anti-apoptotic and proangiogenic activities

miRNA transcriptional profiling of EVs secreted by CPCs or fibroblasts identified several miRNAs that were enriched in the former, such as miR-210, miR-132, miR-146a-3p, and miR-181 (see Supplementary material online, *Figure S3*). Functional roles were studied for two of them: miR-210 and miR-132. Both of these miRNAs inhibited apoptosis in HL-1 cardiomyocytic cells (*Figure 5A*). Conversely, transcriptional silencing of miR-210 exacerbated apoptosis (a similar trend was observed for miR-132). The effect of miR-210 was associated with functional downregulation of its known targets, ephrin A3 and PTP1, but not FLASH/CASP8AP2 (*Figure 5B* and *C*). miR-132 promoted tube formation in HUVECs (*Figure 5D*). This effect was associated with functional downregulation of its known target, RasGap-p120 (*Figure 5E* and *F*). These

results demonstrate that EVs secreted by CPCs are enriched in miRNAs with anti-apoptotic and proangiogenic activities. These miRNAs include miR-210 and miR-132.

## 3.5 EVs secreted by CPCs improve cardiac function after MI *in vivo*

Functional effects of EVs secreted by CPCs were assessed using an *in vivo* model of acute MI. Echocardiographic data are shown in *Figure 6*. Heart rate was similar with all treatments (not shown). Each group of operated rats showed decreased LVEF, both at baseline and at 7 days, compared with sham-operated animals. LVEF at baseline was comparable in all groups except sham-operated animals. In PBS-injected hearts, LVEF significantly decreased from baseline to day 7. Infarcted hearts injected with either dosage of EVs secreted by CPCs, but not those injected with EVs secreted by fibroblasts, showed a higher LVEF at 7 days compared with the PBS-injected control group ($P < 0.05$). LVEF decreased from baseline to Day 7 in hearts injected with PBS, EV-F, or the lower dosage of EV-CPC, whereas it slightly increased in those injected with the higher dosage of EV-CPC (0.8 ± 6.8 vs. $-21.3 \pm 4.5\%$ in the PBS group; $P < 0.05$). The increase in LV diameters observed by Day 7 in the PBS and EV-F groups was prevented by either dosage of EV-CPCs. Systolic LV wall thickening in the infarct border zone was enhanced with either dosage of EV-CPC ($P < 0.05$), but not with EV-F. These results indicate that EVs secreted by CPCs, but not those secreted by fibroblasts, improve cardiac function after MI.

## 3.6 EVs secreted by CPCs inhibit cardiomyocyte apoptosis, reduce scar, and promote angiogenesis after MI

We analysed the morphological consequences of EV injection on scarred areas, cardiomyocyte apoptosis, and blood vessel density in infarcted hearts. Histological analyses showed significantly larger areas of viable tissue in the infarct zone in hearts injected with the higher or lower dosage of EVs secreted by CPCs (41 ± 8 and $32 \pm 5\%$, respectively), compared with those receiving EVs secreted by fibroblasts ($24 \pm 1\%$; $P < 0.05$) or PBS control medium ($23 \pm 2\%$; $P < 0.05$; *Figure 7A* and *B*). Reciprocally, scarred areas were decreased in hearts injected with the higher dosage of EVs from CPCs (59 ± 8 vs. $77 \pm 2\%$ in the PBS group; $P < 0.05$; *Figure 7A* and *C*). TUNEL-positive apoptotic cardiomyocytes were significantly decreased ($P < 0.05$; *Figure 7D*), while blood vessel density being increased in hearts injected with EVs secreted by CPCs (84 ± 13 vs. 34 ± 5 vessel per mm^2 in the PBS group; $P < 0.01$; *Figure 7E*). These findings demonstrate structural benefits of EVs secreted by CPCs and delivered to injured hearts *in vivo*.

4. Discussion

Recent evidence suggests that CPC transplantation into damaged hearts may be beneficial, and that indirect mechanisms may be responsible for most of the therapeutic benefit. Because EVs are increasingly emerging as the active component of the paracrine secretion by various cell types,[17,18] we have investigated their potential role as mediators of the cardioprotective effect of human CPCs. Here, we show that EVs fully account for the cardioprotective and proangiogenic paracrine activities of human CPCs. Indeed, CM-CPC depleted of EVs lacked these activities, which were recapitulated by purified EVs. This observation would imply negligible roles for soluble factors secreted by CPCs,
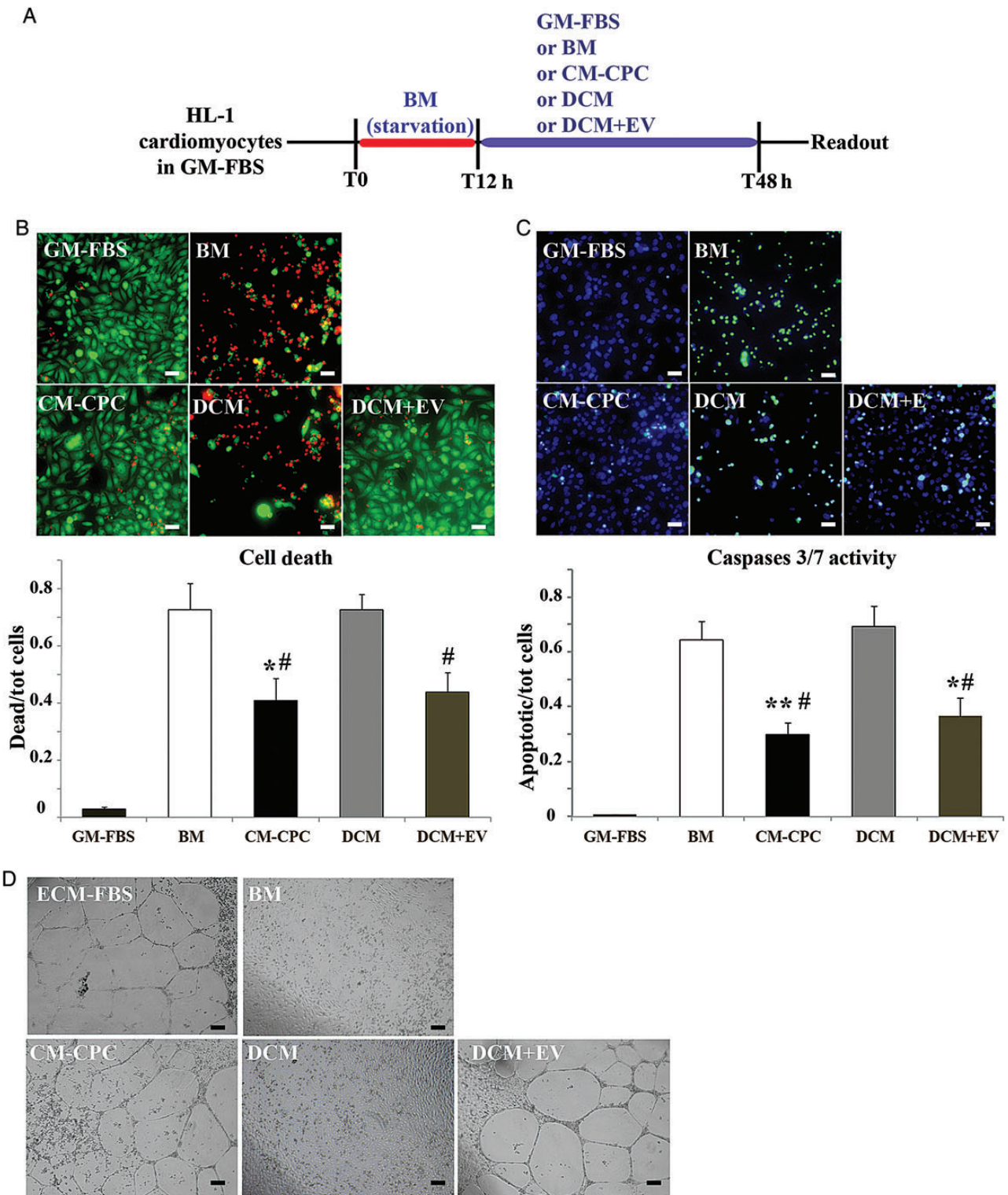
Figure 2 (A) *In vitro* apoptosis assay protocol: in HL-1 cardiomyocytic cell cultures, growth medium (GM-FBS) was changed to serum-free basal medium (BM) at T0. After 12 h starvation (T12 h), BM was either replaced by GM-FBS (control) or supplemented with one of the followings: CM-CPC, CPC-conditioned medium; DCM, EV-depleted CM; or DCM + EV, DCM reconstituted with the previously removed EV fraction. (B) Dead (red) and viable cells (green) in the different study groups. (C) Immunostaining for activated caspase 3/7 (green); nuclear counterstaining with DAPI (blue). Quantitative data are fractions (mean ± SEM) of dead and activated caspase 3/7-positive cells ($n = 4$ experiments; *$P < 0.05$ vs. BM; **$P < 0.01$ vs. BM; #$P < 0.05$ vs. DCM using the parametric Tukey–Kramer multiple comparison test). (D) *In vitro* angiogenesis assay. Photomicrographs showing tube formation in HUVECs under the above conditions (ECM-FBS, endothelial cell medium; reference bars, 0.1 mm).
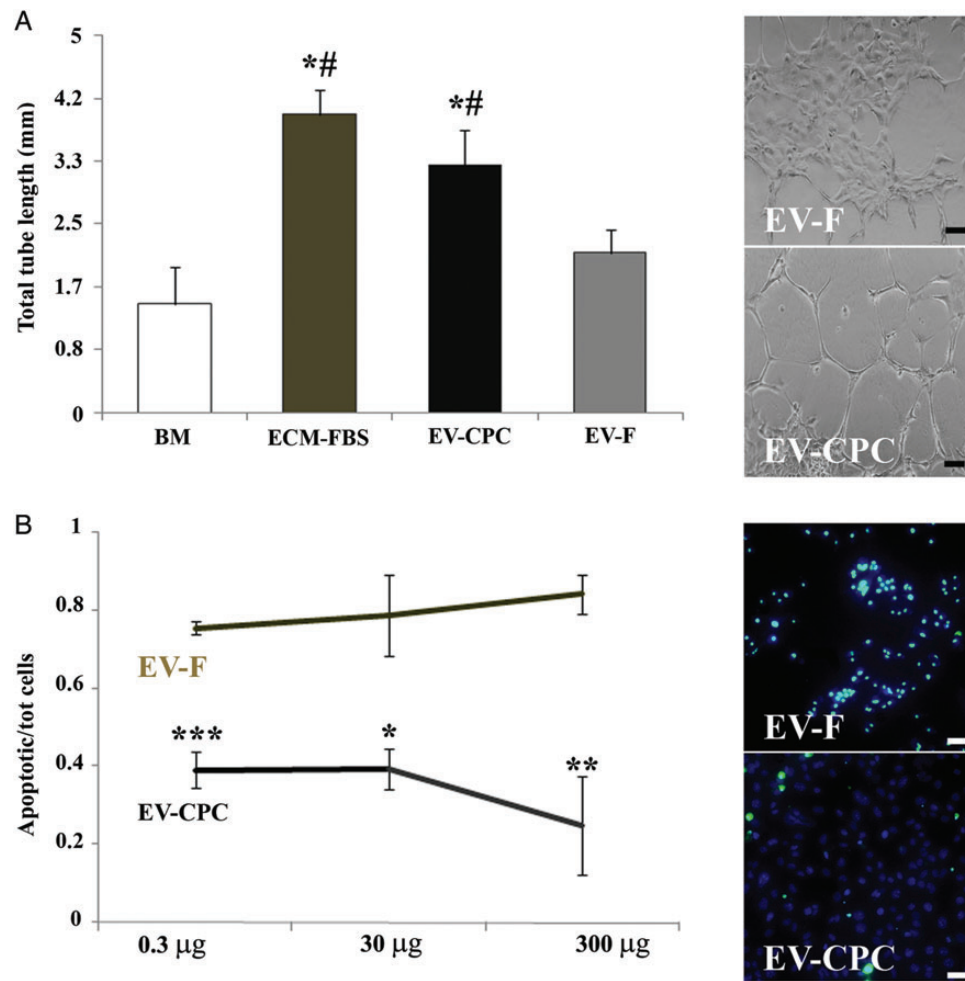
Figure 3 (*A*) *In vitro* angiogenesis assay using purified EVs. EVs secreted by CPCs (EV-CPC) promote endothelial tube formation, whereas those secreted by fibroblasts (EV-F) do not (mean ± SEM; $n = 7$ experiments; *$P < 0.05$ vs. BM; #$P < 0.05$ vs. EV-F using the parametric Tukey−Kramer multiple comparison test; ECM-FBS, endothelial cell medium). (*B*) *In vitro* apoptosis assay using serial dilutions of purified EV-CPV and EV-F, showing dose-dependent inhibition of apoptosis by EV-CPV, but not EV-F. Quantitative data are fractions of the HL-1 cardiomyocytic cells staining positive for activated caspase-3/7 (mean ± SEM; $n = 4$ experiments; *$P < 0.05$; **$P < 0.01$; ***$P < 0.001$ vs. EV-F using the parametric Student's *t*-test; reference bars, 0.1 mm).

such as growth factors and cytokines, which are not encapsulated in membrane vesicles, possibly due to enzymatic degradation in the extracellular compartment. In contrast, membrane vesicles protect their cargoes and deliver them to recipient cells.

Collectively, transmission electron microscopy, nanoparticle tracking analysis, and surface antigen expression data indicated that the purified particles from human CPCs predominantly consists of exosomes. Taking into account the presence of particles >90 nm in diameter in the purified preparations, however, we refer to them as EVs, which encompasses both exosomal and non-exosomal EVs. It should be stressed that many studies of 'exosomes' have actually used heterogeneous EV populations. One notable exception was the study by Lai *et al.*,[18] who purified exosomes secreted by MSCs as a homogeneous population of particles with a hydrodynamic radius of 55−65 nm by size-exclusion fractionation on a HPLC. These particles reduced infarct size in an *ex vivo* mouse Langendorff heart model of myocardial ischaemia/reperfusion injury.

When injected into the infarct border zone *in vivo*, purified EVs secreted by CPCs mitigated cardiomyocyte apoptosis, augmented blood vessel density, reduced scar while increasing viable areas in the infarct zone, and improved cardiac function compared with hearts injected with control medium. In contrast, purified EVs secreted by dermal fibroblasts lacked therapeutic benefits, illustrating the critical role of the parent cell. These findings are in line with, and expand, the aforementioned data by Lai *et al.*[18] on exosomes secreted by MSCs, as well as data by Chen *et al.*,[19] showing anti-apoptotic activity of exosomes secreted by mouse CPCs in a myocardial model of ischaemia/reperfusion injury.

EVs secreted by CPCs were enriched in several miRNAs including miR-210, miR-132, and miR-146a-3p compared with those secreted by fibroblasts. Both miR-210 and miR-132 inhibited apoptosis in the HL-1 cardiomyocytic cell line *in vitro*. This effect of miR-210 was associated with functional down-regulation of its validated targets, ephrin A3 and PTP1, but not of FLASH/CASP8AP2. These results are in line with previous findings.[21] Moreover, miR-132 stimulated tube formation in HUVECs. This effect was associated with functional down-regulation of the known miR-132 target, RasGap-p120. This observation is in agreement with previous data.[22] We also documented dose- and
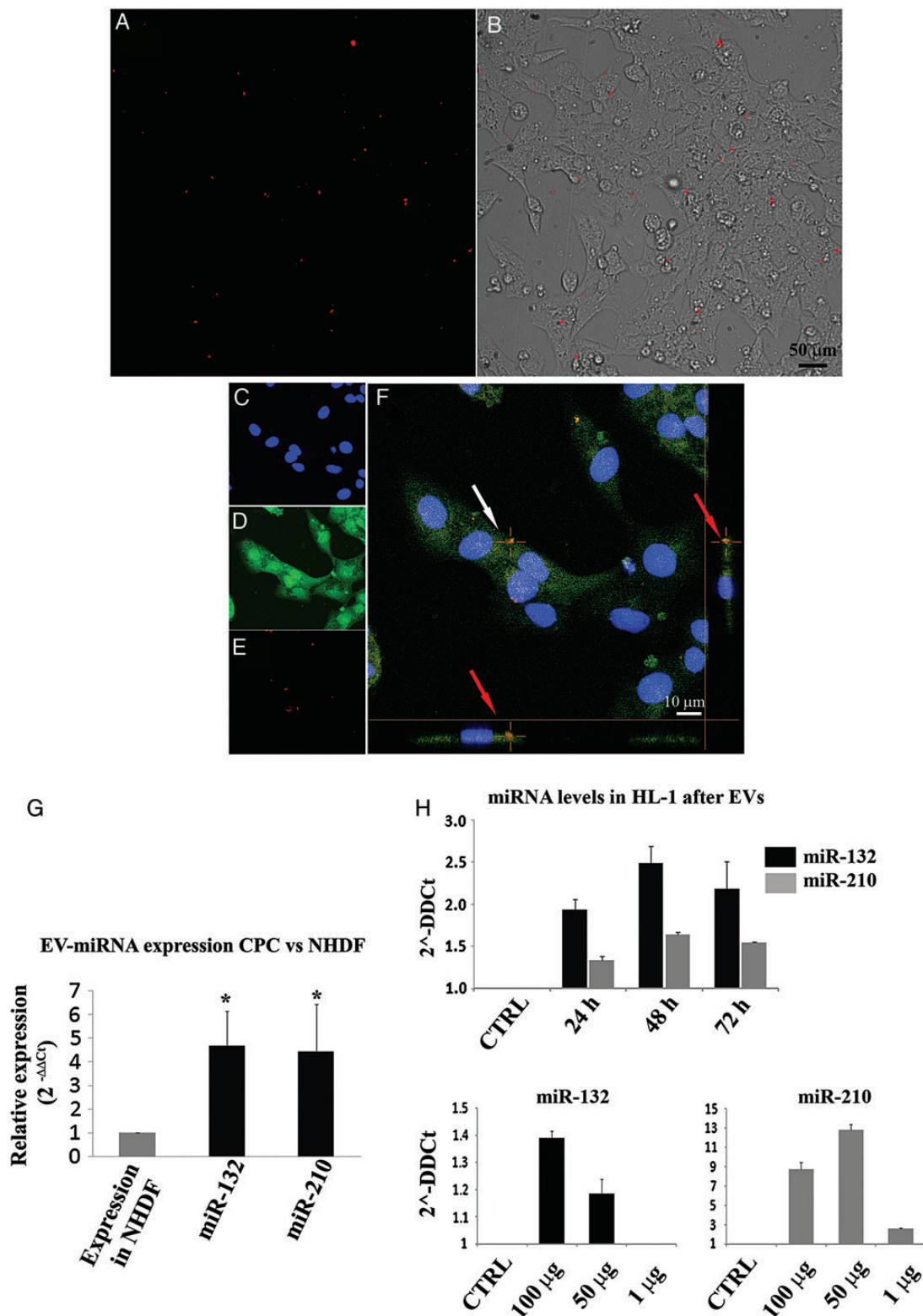
Figure 4 Uptake of EVs from CPCs (EV-CPC) by HL-1 cardiomyocytic cells and changes in the intracellular concentrations of some of the miRNAs enriched in EV-CPC. (*A* and *B*) Fluorescence/light photomicrographs of DiI-labelled EV-CPC (red dots) taken up by cardiomyocytic cells. (*C*) Laser confocal photomicrograph showing DAPI-stained nuclei (blue). (*D*) Cells visualized with calcein (green). (*E*) DiI-labelled EV-CPC (red dots). (*F*) High-magnification merge (white arrow indicates an intracellular EV-CPC aggregate; red arrows indicate the same EV-CPC aggregate depicted in two orthogonal axes, verifying its intracellular location on both axes). (*G*) Relative expression of miR-210 and miR-132 in EV-CPC compared with EV-F (mean $\pm$ SEM; $n = 6$ experiments; *$P < 0.05$ using the parametric Tukey−Kramer multiple comparison test). (*H*)Intracellular concentrations of miR-210 and miR-132 in HL-1 cells exposed to EV-CPC (100 μg of total protein) for the indicated periods of time (upper panel; $n = 3$ experiments). Lower panels: Dose−response studies (measurements at 48 h; $n = 3$ experiments).
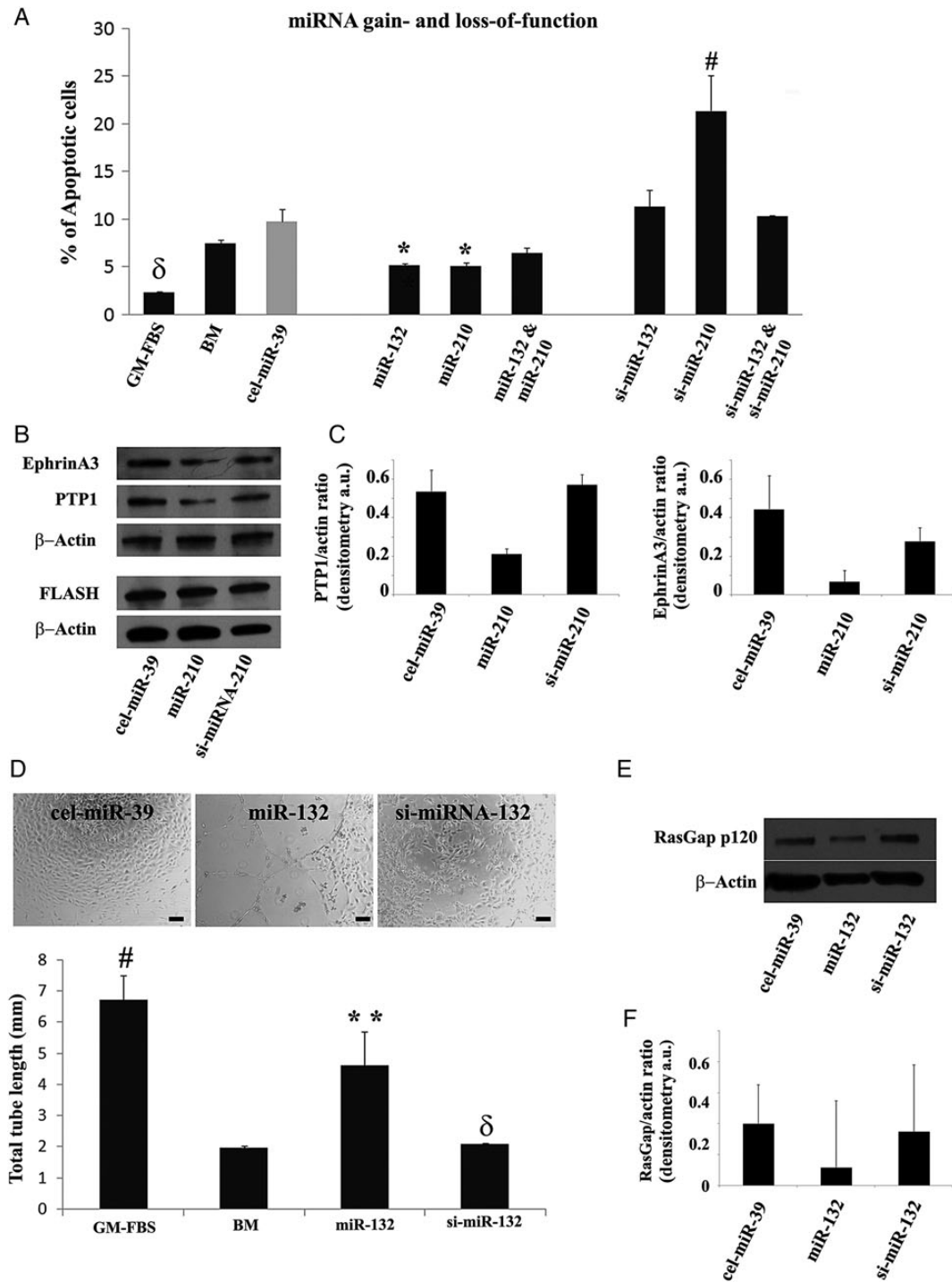
Figure 5 Gain- and loss-of-function studies of miR-210 and miR-132, and regulation of known targets thereof. (A) Apoptotic HL-1 cardiomyocytic cells transfected with a miR-210 and/or a miR-132 mimic, or transcriptional inhibitors thereof (si-miR-210 and si-miR-132; mean $\pm$ SEM; $n = 5$ experiments; *$P < 0.05$ vs. cel-miR-39; #$P < 0.05$ vs. BM; δ$P < 0.05$ vs. BM and cel-miR-39 using non-parametric Dunn's multiple comparisons test). (B) Western blots for the miR-210 targets, ephrin A3, PTP1, and FLASH. (C) Densitometric analysis for PTP1 and ephrin A3 ($n = 3$ experiments; a.u. = arbitrary units). (D) *In vitro* angiogenesis assay. Photomicrographs showing increased tube formation in HUVECs transfected with a miR-132 mimic, but not with si-miR-132 (mean $\pm$ SEM; $n = 6$ experiments; **$P < 0.01$ vs. BM; #$P < 0.05$ vs. miR-132; δ$P < 0.01$ vs. miR-132 using the parametric Tukey–Kramer multiple comparison test; dimensional bars, 100 μm). (E) Western blot for RasGap-p120. (F) Densitometric analysis of RasGap-p120 ($n = 3$ experiments; a.u. = arbitrary units).

time-dependent increases in the intracellular concentrations of miR-210 and miR-132 after exposure of the HL-1 cardiomyocytic cell line to EVs secreted by CPCs. This finding shows that purified donor EVs can modify miRNA concentrations in recipient cardiomyocytes. miRNA transfer therefore appears to be a plausible mechanism for the therapeutic benefit of EVs.
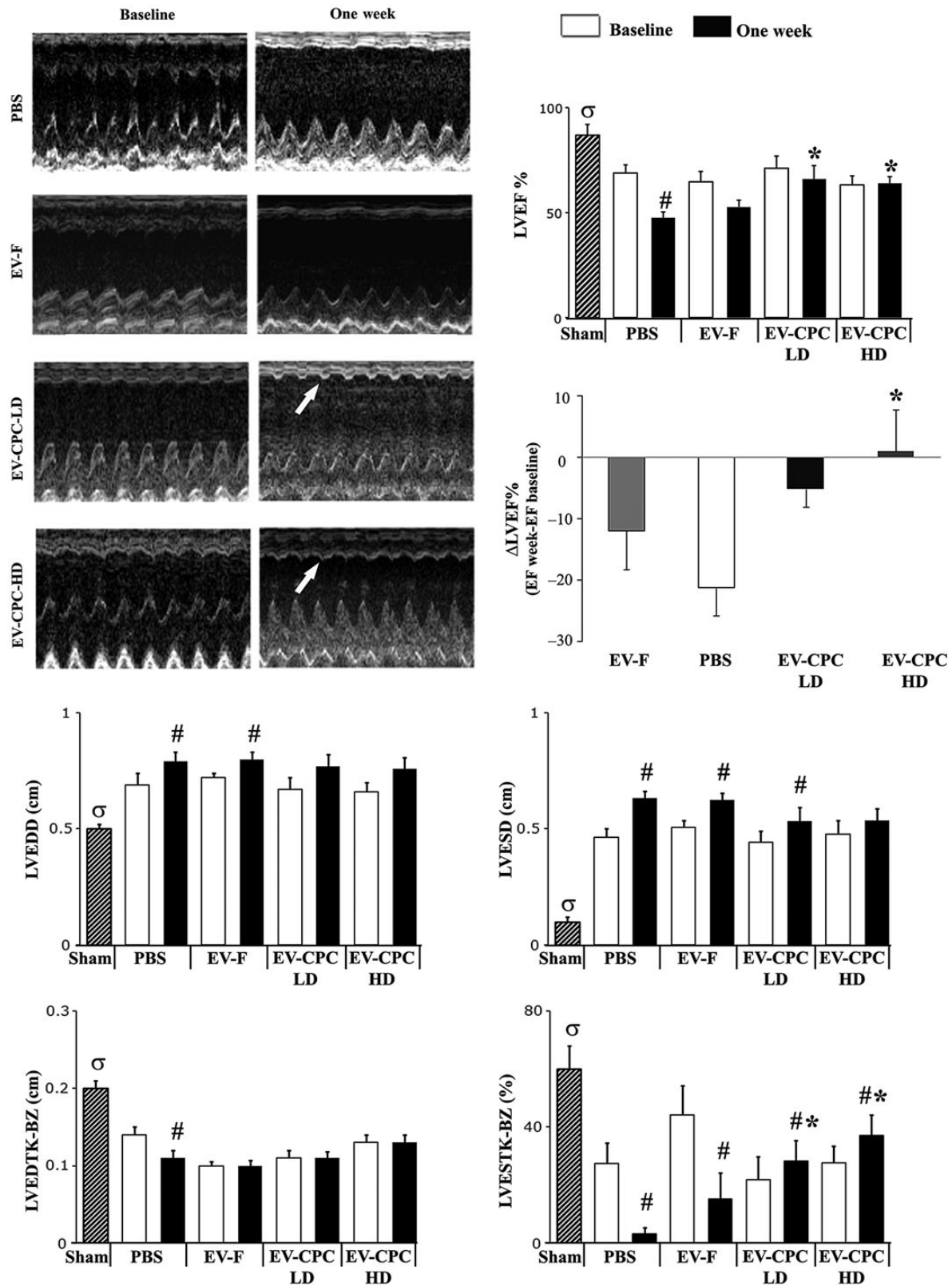
Figure 6 Echocardiographic results at baseline (i.e. Day 2; white bars) and at Day 7 after MI (black bars). M-mode images in the different groups at Day 7 (white arrows indicate systolic anterior wall thickening in EV-CPC−injected hearts). Changes in LVEF from baseline to Day 7 were negative in all groups, but in hearts injected with the higher dosage (HD) in EV-CPC (LD, lower dosage; LVEDD/LVESD, LV end-diastolic/end-systolic diameter; LVEDTHK-BZ, LV end-diastolic wall thickness; LVESTK-BZ, end-systolic wall thickening in the border zone; mean $\pm$ SEM; PBS, $n = 9$; 30 μg EV-CPC LD, $n = 9$; 300 μg EV-CPC HD, $n = 10$; 300 μg Exo-F, $n = 4$; sham, $n = 9$; *$P < 0.05$ vs. PBS; #$P < 0.05$ at Day 7 vs. baseline; $^\sigma P < 0.05$ sham vs. PBS at Day 7 using the parametric Tukey−Kramer multiple comparison test).
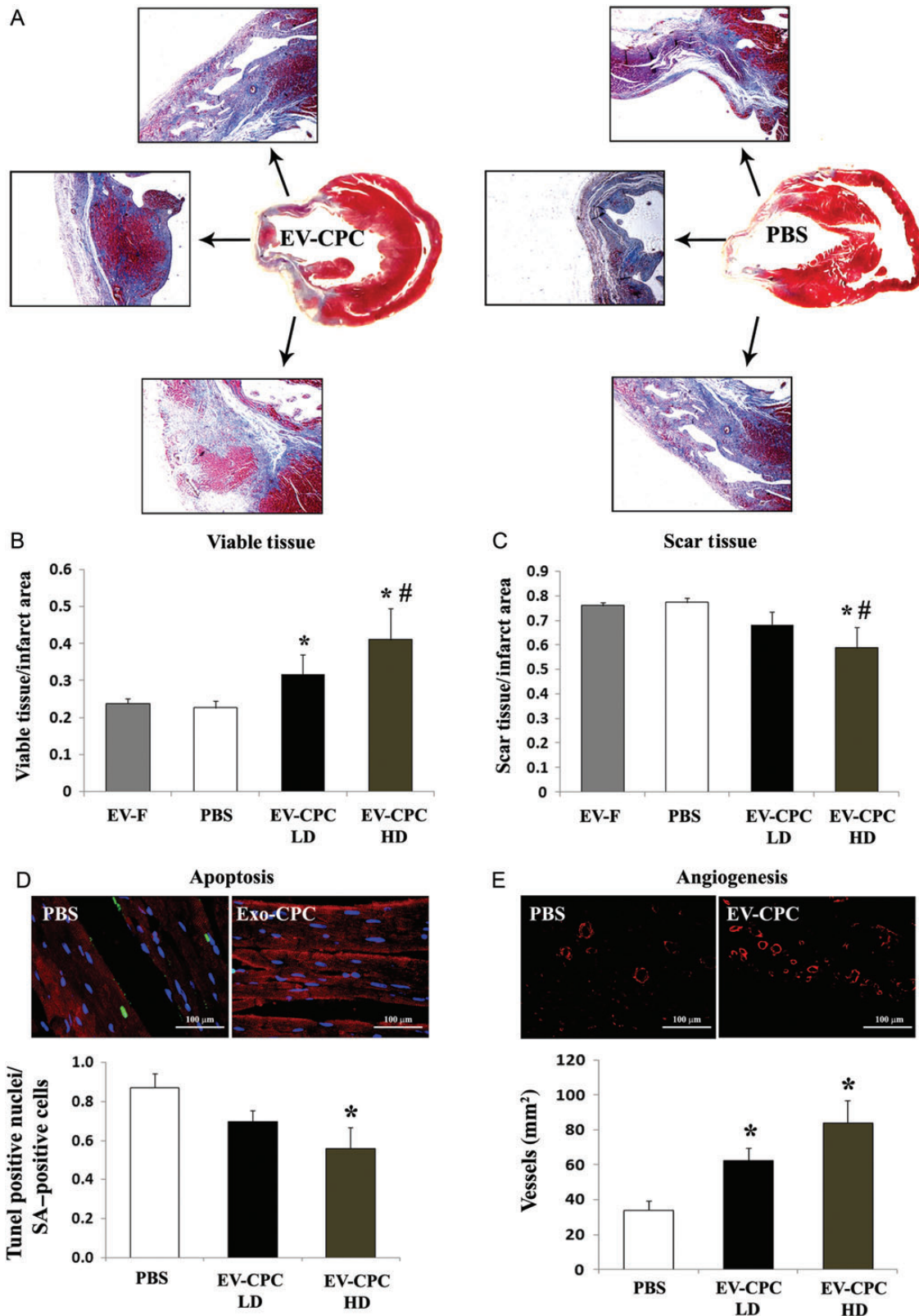
Figure 7 Morphometric analyses of infarcted rat hearts. (*A*) Masson's trichrome-stained sections of EV-CPC- (left) and PBS-injected hearts (right). (*B* and *C*) Quantitative analyses of viable and scar areas (%) in the infarct zone. (*D*) TUNEL-positive (green) apoptotic cardiomyocytes (α-SA -positive cells; red). (*E*) Smooth muscle actin-positive blood vessels (red). Quantitative analyses of apoptotic cardiomyocytes and vessel density (mean $\pm$ SEM; EV-F, $n = 4$; all other groups, $n = 5$; HD/LD, higher/lower dosage of EV-CPC; $*P < 0.05$ vs. PBS; $^{\#}P < 0.05$ vs. EV-F using the parametric Tukey−Kramer multiple comparison test).

As cell-free products, EVs including exosomes may have a potential for circumventing many of the limitations of using replicating cells as therapeutic agents.[29] Indeed, secreted vesicles may be easier to manufacture and standardize in terms of dosage and biological activity compared with their parent cells. Exosomes are stable during storage at $-20°C$, and their size is unaffected by multiple freezing to $-20°C$ and thawing, whereas it decreases at 4 and 37°C, indicating structural changes or degradation.[30] After all, there may be no interest in transplanting cells that essentially act through their paracrine secretion. Further studies are needed to address long-term effects of exosome therapy for damaged hearts and whether allogeneic cells could be used as EV donors for clinical use.

In conclusion, we have demonstrated that EVs are the active component of the paracrine secretion by human CPCs, are enriched in miRNAs with anti-apoptotic and proangiogenic activities, and can improve cardiac function after MI.

Supplementary material

Supplementary material is available at *Cardiovascular Research online*.

References

1. Schächinger V, Erbs S, Elsässer A, Haberbosch W, Hambrecht R, Hölschermann H, Yu J, Corti R, Mathey DG, Hamm CW, Süselbeck T, Assmus B, Tonn T, Dimmeler S, Zeiher AM; REPAIR-AMI Investigators. Intracoronary bone marrow-derived progenitor cells in acute myocardial infarction. *N Engl J Med* 2006;**355**:1210−1221.

2. Houtgraaf JH, den Dekker WK, van Dalen BM, Springeling T, de Jong R, van Geuns RJ, Geleijnse ML, Fernandez-Aviles F, Zijlsta F, Serruys PW, Duckers HJ. First experience in humans using adipose tissue-derived regenerative cells in the treatment of patients with ST-segment elevation myocardial infarction. *J Am Coll Cardiol* 2012;**59**:539−540.

3. Menasché P, Alfieri O, Janssens S, McKenna W, Reichenspurner H, Trinquart L, Vilquin JT, Marolleau JP, Seymour B, Larghero J, Lake S, Chatellier G, Solomon S, Desnos M, Hagège AA. The Myoblast Autologous Grafting in Ischemic Cardiomyopathy (MAGIC) trial: first randomized placebo-controlled study of myoblast transplantation. *Circulation* 2008;**117**:1189−1200.

4. Makkar RR, Smith RR, Cheng K, Malliaras K, Thomson LE, Berman D, Czer LS, Marbán L, Mendizabal A, Johnston PV, Russell SD, Schuleri KH, Lardo AC, Gerstenblith G, Marbán E. Intracoronary cardiosphere-derived cells for heart regeneration after myocardial infarction (CADUCEUS): a prospective, randomised phase 1 trial. *Lancet* 2012; **379**:895−904.

5. Marbán E, Malliaras K. Mixed results for bone marrow−derived cell therapy for ischemic heart disease. *JAMA* 2012;**308**:2405−2406.

6. Messina E, De Angelis L, Frati G, Morrone S, Chimenti S, Fiordaliso F, Salio M, Battaglia M, Latronico MV, Coletta M, Vivarelli E, Frati L, Cossu G, Giacomello A. Isolation and expansion of adult cardiac stem cells from human and murine heart. *Circ Res* 2004;**95**:911−921.

7. Smith RR, Barile L, Cho HC, Leppo MK, Hare JM, Messina E, Giacomello A, Abraham MR, Marbán E. Regenerative potential of cardiosphere-derived cells expanded from percutaneous endomyocardial biopsy specimens. *Circulation* 2007;**115**:896−908.

8. Chimenti I, Smith RR, Li TS, Gerstenblith G, Messina E, Giacomello A, Marbán E. Relative roles of direct regeneration versus paracrine effects of human cardiosphere-derived cells transplanted into infarcted mice. *Circ Res* 2010;**106**:971−980.

9. Duran JM, Makarewich CA, Sharp TE, Starosta T, Zhu F, Hoffman NE, Chiba Y, Madesh M, Berretta RM, Kubo H, Houser SR. Bone-derived stem cells repair the heart after

myocardial infarction through transdifferentiation and paracrine signaling mechanisms. *Circ Res* 2013;**113**:539−552.

10. Li TS, Cheng K, Malliaras K, Smith RR, Zhang Y, Sun B, Matsushita N, Blusztajn A, Terrovitis J, Kusuoka H, Marbán L, Marbán E. Direct comparison of different stem cell types and subpopulations reveals superior paracrine potency and myocardial repair efficacy with cardiosphere-derived cells. *J Am Coll Cardiol* 2012;**59**:942−953.

11. Timmers L, Lim SK, Arslan F, Armstrong JS, Hoefer IE, Doevendans PA, Piek JJ, El Oakley RM, Choo A, Lee CN, Pasterkamp G, de Kleijn DP. Reduction of myocardial infarct size by human mesenchymal stem cell conditioned medium. *Stem Cell Res* 2007; **1**:129−137.

12. Mathivanan S, Ji H, Simpson RJ. Exosomes: extracellular organelles important in intercellular communication. *J Proteomics* 2010;**73**:1907−1920.

13. Thery C. Exosomes: secreted vesicles and intercellular communications. *F1000 Biol Rep* 2011;**3**:15.

14. Valadi H, Ekstrom K, Bossios A, Sjostrand M, Lee JJ, Lotvall JO. Exosome-mediated transfer of mRNAs and microRNAs is a novel mechanism of genetic exchange between cells. *Nat Cell Biol* 2007;**9**:654−659.

15. Stoorvogel W. Functional transfer of microRNA by exosomes. *Blood* 2012;**119**: 646−648.

16. Bobrie A, Colombo M, Krumeich S, Raposo G, Théry C. Diverse subpopulations of vesicles secreted by different intracellular mechanisms are present in exosome preparations obtained by differential ultracentrifugation. *J Extracell Vesicles* 2012;**1**:18397.

17. Sahoo S, Klychko E, Thorne T, Misener S, Schultz KM, Millay M, Ito A, Liu T, Kamide C, Agrawal H, Perlman H, Qin G, Kishore R, Losordo DW. Exosomes from human CD34(+) stem cells mediate their proangiogenic paracrine activity. *Circ Res* 2011;**109**: 724−728.

18. Lai RC, Arslan F, Lee MM, Sze NS, Choo A, Chen TS, Salto-Tellez M, Timmers L, Lee CN, El Oakley RM, Pasterkamp G, de Kleijn DP, Lim SK. Exosome secreted by MSC reduces myocardial ischemia/reperfusion injury. *Stem Cell Res* 2010;**4**:214−222.

19. Chen L, Wang Y, Pan Y, Zhang L, Shen C, Qin G, Ashraf M, Weintraub N, Ma G, Tang Y. Cardiac progenitor-derived exosomes protect ischemic myocardium from acute ischemia/reperfusion injury. *Biochem Biophys Res Commun* 2013;**431**:566−571.

20. Barile L, Gherghiceanu M, Popescu LM, Moccetti T, Vassalli G. Ultrastructural evidence of exosome secretion by progenitor cells in adult mouse myocardium and adult human cardiospheres. *J Biomed Biotechnol* 2012;**2012**:354605.

21. Hu S, Huang M, Li Z, Jia F, Ghosh Z, Lijkwan MA, Fasanaro P, Sun N, Wang X, Martelli F, Robbins RC, Wu JC. MicroRNA-210 as a novel therapy for treatment of ischemic heart disease. *Circulation* 2010;**122**:S124−S131.

22. Katare R, Riu F, Mitchell K, Gubernator M, Campagnolo P, Cui Y, Fortunato O, Avolio E, Cesselli D, Beltrami AP, Angelini G, Emanueli C, Madeddu P. Transplantation of human pericyte progenitor cells improves the repair of infarcted heart through activation of an angiogenic program involving micro-RNA-132. Novelty and significance. *Circ Res* 2011; **109**:894−906.

23. Hinescu ME, Gherghiceanu M, Suciu L, Popescu LM. Telocytes in pleura: two- and three-dimensional imaging by transmission electron microscopy. *Cell Tissue Res* 2011;**343**: 389−397.

24. Claycomb WC, Lanson NA Jr, Stallworth BS, Egeland DB, Delcarpio JB, Bahinski A, Izzo NJ Jr. HL-1 cells: a cardiac muscle cell line that contracts and retains phenotypic characteristics of the adult cardiomyocyte. *Proc Natl Acad Sci USA* 1998;**95**:2979−2984.

25. Fasanaro P, D'Alessandra Y, Di Stefano V, Melchionna R, Romani S, Pompilio G, Capogrossi MC, Martelli F. MicroRNA-210 modulates endothelial cell response to hypoxia and inhibits the receptor tyrosine kinase ligand Ephrin-A3. *J Biol Chem* 2008; **283**:15878−15883.

26. Kim HW, Haider HK, Jiang S, Ashraf M. Induction of FLASH/CASP8AP2 in miR-210 knocked-down (PC)MSCs resulted in increased cell apoptosis. Taken together, these data demonstrated that cytoprotection afforded by IP was regulated by miR-210 induction via FLASH/Casp8ap2 suppression. *J Biol Chem* 2009;**284**:33161−33168.

27. Campan M, Lionetti V, Aquaro GD, Forini F, Matteucci M, Vannucci L, Chiuppesi F, Di Cristofano C, Faggioni M, Maioli M, Barile L, Messina E, Lombardi M, Pucci A, Pistello M, Recchia FA. Ferritin as a reporter gene for in vivo tracking of stem cells by 1.5-T cardiac MRI in a rat model of myocardial infarction. *Am J Physiol Heart Circ Physiol* 2011;**300**:H2238−H2250.

28. Zentilin L, Puligadda U, Lionetti V, Zacchigna S, Collesi C, Pattarini L, Ruozi G, Camporesi S, Sinagra G, Pepe M, Recchia FA, Giacca M. Cardiomyocyte VEGFR-1 activation by VEGF-B induces compensatory hypertrophy and preserves cardiac function after myocardial infarction. *FASEB J* 2010;**24**:1467−1478.

29. Sahoo S, Losordo DW. Exosomes and cardiac repair after myocardial infarction. *Circ Res* 2014;**114**:333−344.

30. Sokolova V, Ludwig AK, Hornung S, Rotan O, Horn PA, Epple M, Giebel B. Characterisation of exosomes derived from human cells by nanoparticle tracking analysis and scanning electron microscopy. *Colloids Surf B Biointerfaces* 2011;**87**:146−150.